Deep Low-Frequency Earthquakes Associated with the Eruptions of Shinmoe-dake in Kirishima Volcanoes

Ryo Kurihara[1], Kazushige Obara[1], Akiko Takeo[1], and Yusaku Tanaka[1]

[1] Earthquake Research Institute, the University of Tokyo

Corresponding author: Ryo Kurihara (rkuri@eri.u-tokyo.ac.jp)

Key Points:

- Activation of low-frequency earthquakes at depths of 20–27 km started one year before the 2011 eruptions of Shinmoe-dake.
- Waveforms of low-frequency earthquakes associated with the 2011 eruptions indicate lower dominant frequencies than those of the others.
- Activated low-frequency earthquake locations might have been switched by fluid path redistribution with eruption style transitions.

Abstract

Deep low-frequency (DLF) earthquakes occur beneath the Kirishima volcanoes in southwest Japan at depths of 10–30 km. In this study, we aim to reveal the relationship between DLF earthquakes and volcanic activity including eruptions by relocating the hypocenters of the earthquakes using the network correlation coefficient method and detecting the earthquakes comprehensively using the matched filter technique. Hypocenters of DLF earthquakes are found to be concentrated in some separated small clusters within depths of 10–15 and 20–27 km. Activation of deeper DLF earthquakes had been observed for approximately two years from December 2009, during which various styles of eruptions occurred. Such a two-year increase in DLF seismicity was well correlated with crustal deformation because of the volume change of a magma reservoir. The waveforms and hypocenters of DLF earthquakes during the activation period were different from those during other time periods. The activated DLF earthquakes mostly had low dominant frequencies and were located in four deeper clusters. The activation of each cluster was switched three times at the transition of the eruption styles. These results suggest that DLF earthquakes might occur near magma sills and could be triggered by fluid flow in the changing paths by complex eruption processes. In addition, the waveforms and hypocenters of DLF earthquakes associated with the 2018 eruptions are different from those associated with the 2011 eruptions. The fluid paths of the 2018 eruptions might be different from those of the 2011 eruptions.

Plain Language Summary

Deep low-frequency (DLF) earthquakes occur at depths of 10–30 km beneath the Kirishima volcanoes, which is one of the most active volcanoes in Japan. In the last decade, two major series of eruptions were observed there. The relationship between DLF earthquakes and volcanic activity such as eruptions is still unknown; therefore, we conduct two analyses, namely, relocation and detection to obtain the precise spatial distribution and comprehensive temporal distribution of DLF earthquakes based on waveform correlations. The result is that DLF earthquakes occurred in some small clusters, having been activated for approximately two years from December 2009, during which various styles of eruptions including subplinian eruptions on 26–27 January 2011 occurred. The long-term increase in DLF earthquakes was well correlated with crustal deformation because of the volume change of the magma reservoir. Most DLF earthquakes associated with the 2011 eruptions are distributed in four deeper clusters which are different from those of DLF earthquakes in the other time periods. Moreover, the clusters were switched three times, which approximately correlates with the transitions of eruption styles. These results suggest that DLF earthquakes were triggered by fluid flow in the deep crust related to the eruptions.

1 Introduction

We frequently observe anomalous microearthquakes with predominant frequencies of 1–10 Hz at depths of around 30 km in the Japan island arc whereas most of all the inland regular earthquakes occur at depths shallower than 15 km. The earthquakes are usually called as deep low-frequency (DLF) earthquakes. Japan meteorology agency (JMA) observes the DLF earthquakes, and the earthquakes are included in the seismic catalog of JMA [Katsumata and Kamaya, 2003]. The depth of 30 km for many DLF earthquakes is equivalent to the Moho discontinuity [Ukawa, 2007; Kosuga et al., 2017]; however, low-frequency earthquakes sometimes occur at depths from 10 to 50 km. In this study, we define low-frequency earthquakes deeper than 10 km as DLF earthquakes. DLF earthquakes are classified into three types based on their locations: tectonic DLF earthquakes occurring at plate subduction zones, volcanic DLF earthquakes occurring near volcanoes, and semi-volcanic DLF earthquakes occurring far from either of those [Aso et al., 2013]. Regardless of their location, waveforms of DLF earthquakes are similar to each other.

DLF earthquakes distributed near volcanoes can be a key to reveal the physical processes of volcanic activity, including eruptions, because DLF earthquake activity is supposed to be associated with eruptions. Ukawa and Ohtake [1987] reported that a DLF earthquake at a depth of approximately 30 km occurred before the 1986 eruption of Izu-Oshima volcano, Japan. White [1996] showed that DLF earthquakes occurred before the 1991 eruption of Pinatubo volcano, Philippines. Shapiro et al. [2017] and Frank et al. [2018] showed the relationship between DLF and long-period earthquakes near the surface beneath the Klyuchevskoy volcano group at Kamchatka, Russia. However, the relationship is still unknown in many other volcanoes. Takahashi and Miyamura [2009] analyzed DLF earthquakes all over Japan based on the JMA catalog and concluded that they could not find DLF earthquakes corresponding to surface volcanic activity such as eruptions.

DLF earthquakes are considered to be affected by fluid movements in a volcanic area [Aki and Koyanagi, 1981; Hensch et al., 2019]. DLF earthquakes occur around the low velocity and low Q zones possibly because of the existence of fluid [Hasegawa et al., 2005]. At Laacher See volcano in Germany, migration of magma or magmatic fluid may be related to DLF earthquakes and it suggests recharge of magma chamber [Hensch et al., 2019]. Hotovec-Ellis et al. [2018] reported similar results derived at Mammoth Mountain California, USA. The above fluid model is supported by studies on focal mechanisms of DLF earthquakes. Nakamichi et al. [2003] revealed that DLF earthquakes at Iwate volcano in northeastern Japan have focal mechanisms including compensated-linear-vector-dipole (CLVD) components, which suggests existence of fluid movement. Aso and Tsai [2014] proposed the cooling magma model in which DLF earthquakes are considered to be triggered by thermal strain.

Kirishima volcanoes located in the southern part of Kyushu island includes three active volcanoes—Shinmoe-dake, Io-yama, and Ohachi. Shinmoe-dake has been one of the most active volcanoes in Japan over the past few decades. In fact, it erupted several times in 2008–2011 and 2017–2018. Phreatic eruptions as precursory activity occurred in 2008–2010 [Suzuki et al., 2013], subplinian eruptions occurred on 26–27 January 2011, vulcanian eruptions occurred in February and April 2011, and phreatomagmatic eruptions occurred from June to September 2011 [Nakada et al., 2013]. Io-yama, located northwest of Shinmoe-dake, erupted in October 2017 and March–April 2018 as well [Japan Meteorology Agency, 2018]. In Kirishima volcanoes, volcanic DLF earthquakes occur at depths of approximately 10–15 km and 20–27 km, according to the JMA catalog. In the vicinity of these DLF earthquakes, low velocity zones at depths of 5–15 and 25–35 km have been imaged by tomography and seismic interferometry [Yamamoto and Ida, 1994; Nagaoka et al., 2018; Zhao et al., 2018]. However, DLF seismicity associated with eruptions has not been observed in Kirishima volcanoes up to now.

We aim to reveal the relationship between DLF earthquakes and volcanic activity in this study. For this purpose, precise locations of DLF earthquakes and a comprehensive catalog of earthquakes are necessary. However, the JMA catalog includes errors of locations, which make it insufficient for that purpose, because the waveforms of the DLF earthquake are complicated, and the onsets of P and S waves are unclear. Thus, to obtain precise locations and a comprehensive catalog of DLF earthquakes, we use the network correlation coefficient method [Ohta and Ide, 2011] and the matched filter technique [Gibbons and Ringdal, 2006; Shelly et al., 2007]. Then, we show the results of the analyses, indicating increases in DLF earthquakes associated with eruptions in Kirishima volcanoes. In addition, we classify DLF earthquakes and find characteristic types of DLF earthquakes which mainly occur with eruptions.

2 Data and Methods

In this study, we use the network correlation coefficient (NCC) method and the matched filter technique (MFT). For both analyses, we use three-component seismograms of the high-sensitivity seismograph network (Hi-net), operated by the National Research Institute for Earth Science and Disaster Resilience (NIED) [Okada et al., 2004; NIED, 2019] after applying a band-pass filter of 1−4 Hz.

To relocate the hypocenters of DLF earthquakes in the JMA catalog, we adapt the NCC method, which was originally used for tectonic DLF earthquakes in the Nankai subduction zone [Ohta and Ide, 2011]. NCC refers to the summed correlation coefficients between two waveforms of one earthquake pair calculated over many stations. In this method, the relative locations of each earthquake pair are estimated by maximizing the NCC on a grid search. We use the 100-Hz sampling data of velocity waveforms observed at 10 Hi-net stations (Figure 1). We apply this method to all of the 275 DLF earthquakes that occurred from April 2004 to December 2015 in the JMA catalog. The length of the time window is 5 s, and the estimated arrival time is at the center of the time window. Estimated arrival time is calculated by using P- and S-wave velocities for vertical and horizontal components, respectively. To reduce error in the locations, we exclude the earthquakes whose correlations between them and the other earthquakes are less than six times the standard deviations of NCCs for various assumptions of relative relocation.

To make a comprehensive catalog of DLF earthquakes, we apply MFT [Gibbons and Ringdal, 2006; Shelly et al., 2007]. In this method, DLF earthquakes are detected when the summed correlation coefficients (CC) of waveforms at many stations are higher than the detection threshold. The period of the analysis is from April 2004 to December 2018. We first decimate the Hi-net data from 100 Hz to 12.5 Hz to reduce the computational cost. Time windows of 5 s are used, and the centers of the time windows correspond to the estimated arrival times of S waves in all components. We select 200 template DLF earthquakes with high signal to noise ratios (SN ratios) from the JMA catalog and use three components of six Hi-net stations, which show high SN ratios. When the data of one or two observation stations are missing for the target day, we add the same amount of data from the other stations that are used for relocation as well. The maximum value of the summed CC is always 18. The detection threshold of summed CC is set to 5.5, equivalent to approximately 11 times of median absolute deviations (MAD). This value is higher than eight times of MAD, used for analysis of tectonic DLF earthquakes [Shelly et al., 2007], to prevent misdetection. After detection, we select the one detected earthquake that has the highest summed CC in 10-s time window to avoid multiple counting of one DLF earthquake.

Regardless of our severe threshold, misdetections sometimes occur because the number of stations is limited, and the SN ratios of waveforms are usually low. To reduce misdetections more, we use CC and estimated magnitudes calculated based on template DLF earthquakes by the following equation

$$Mj_{\mathrm{detect}} = Mj_{\mathrm{temp}} + \frac{1}{0.85}\log\left(\frac{V_{\mathrm{detect}}}{V_{\mathrm{temp}}}\right) \quad \cdot\cdot\cdot (1)$$

where Mj_{detect} and Mj_{temp} are the JMA magnitudes of the detected DLF earthquake and the template earthquake, respectively. V_{detect} and V_{temp} are the maximum values of velocities in the time windows of 5 s. We use three-component data from the N.SUKH station to calculate magnitude. The 0.85 is obtained by the equation used to estimate the magnitude in JMA [Funasaki and Earthquake Prediction Information Division, 2004]. We distinguish detected DLF earthquakes from misdetections based on the following procedure. First, we select as DLF earthquakes only the events whose summed CC are larger than 7.0. Next, we remove those with large magnitudes because they may reflect the surface waves of regular earthquakes. The threshold of the magnitudes is calculated based on the DLF earthquakes selected above. Events are determined as misdetections when the magnitudes of the events with summed CC between 5.5 and 7.0 are larger than the magnitude of the top three percent DLF earthquakes, which is equal to magnitude 0.9. The magnitudes of some events cannot be calculated because the magnitudes of some template earthquakes were not determined by JMA. We do not use the threshold of magnitude for such detected events. Finally, to reduce misdetections by noise such as wind or microseisms, we use the spectrum ratios of 2.0–4.0 Hz to 0.5–1.0 Hz at the N.NRAH station, which shows the highest SN ratio values in the template events. We remove the events whose summed CC are between 5.5 and 7.0 and spectrum ratios are less than 0.2. In other words, we remove the events with large energy on the 0.5–1.0-Hz band, which is lower than the dominant frequency of DLF earthquakes, 1.0–10.0 Hz.

3 Locations of DLF earthquakes

Figure 2a shows the locations of DLF earthquakes in the Kirishima volcanoes in the JMA catalog. One unique characteristic of these earthquakes is that there is a seismic gap at a depth of 15–20 km. In other words, the hypocenters are separated into a shallow spot at a depth of 10–15 km and a deep spot at a depth of 20–27 km, while the hypocenters of DLF earthquakes in most of the other volcanoes have continuous distributions in the vertical direction according to the JMA catalog. Both spots are above the Moho discontinuity in the Kirishima volcanoes at the depth of approximately 30 km here [Matsubara et al., 2017].

We obtain new locations of 201 DLF earthquakes from 275 earthquakes in the JMA catalog by NCC method. Relocated hypocenters are also separated into both shallow and deep spots. Unlike the original catalog of the JMA, the hypocenters are concentrated in some smaller clusters (Figure 2b). In other words, DLF earthquakes are not distributed continuously in the vertical direction but are located in isolated small clusters. Beneath the Ohachi volcano, the hypocenters are concentrated at depths of approximately 12 and 14 km. Most of the DLF earthquakes that occurred deeper than 20 km were concentrated in the largest cluster at a depth of 22 km, while some earthquakes are located in small clusters at depths of 25–27 km. The DLF earthquakes deeper than 20 km are located in the north of Ohachi (Figure 2b).

The errors of the relocation are difficult to estimate because the NCC method does not use the linear equation. However, the errors may be less than few kilometers and we find the difference of DLF seismicity by the depths even if the distance between the earthquakes are smaller than a few kilometers, as discussed in next section.

4 Activities of DLF earthquakes corresponding to the eruptions

4.1 Temporal distribution of DLF earthquakes

From April 2004 to December 2018, 2964 DLF earthquakes were detected by MFT and completeness magnitude of DLF earthquakes was approximately 0.0. Cumulative numbers of DLF earthquakes in the JMA catalog and MFT catalog are shown in Figure 3. DLF earthquakes in the JMA catalog occurred constantly (Figure 3b) but those in the MFT catalog increased significantly between 2010 and 2011 (Figure 3c).

Around the 2011 subplinian eruptions, there are some notable points of DLF activity (Figure 4). First, a small increase in DLF earthquakes started at the end of 2009. Second, there is a step in the cumulative number on August 2010, which reflects a swarm of DLF earthquakes. Third, DLF earthquakes were activated in December 2010. Finally, a swarm of DLF earthquakes occurred in February 2011. However, there is no significant activation of DLF earthquakes directly corresponding to the subplinian eruptions on 26–27 January 2011. After the swarm of DLF earthquakes in February 2011, the long-term increase in DLF earthquakes had gradually finished by the end of 2011. DLF earthquakes are generally separated into two spots shallower and deeper than the depth of 17 km (see Figure 2). Most DLF earthquakes detected by MFT are located in the deeper spot (Figures 3e) while those in the shallower spot number fewer than 200 without significant activations near the 2011 eruptions (Figure 3d).

The seismicity of DLF earthquakes from December 2009 is correlated with crustal deformation. Figures 3a and 4a show the amount of the radial component of horizontal displacement of Ebino relative to Makizono (see Figure 1), calculated from GNSS data (F3 solutions) provided by the Geospatial Information Authority of Japan. These two stations show the largest relative horizontal displacement which probably reflects the volume change in the magma reservoir located near Io-yama (yellow star in Figure 1) at a depth of 8 km [Nakao et al., 2013]. The trend of horizontal displacement also changed at the end of 2009, when DLF earthquakes increased, and the extension trend corresponded to the 2011 eruptions of Shinmoe-dake. The change in the trend lasted until the end of 2011, except for the shortening by the eruptions in January 2011.

After the sequence of DLF earthquakes associated with the 2011 eruptions, another small activation of DLF earthquakes was observed after September 2017 (Figure 3c). This increase is also correlated with the eruptions of Shinmoe-dake and Io-yama that occurred in October 2017 and in March–April 2018. This increase is observed in the JMA catalog as well. The horizontal displacement is also extended in this period.

Most newly detected DLF earthquakes have very small magnitudes. The estimated magnitudes of the earthquakes are between minus 1.0 and 1.0. Therefore, it is difficult to analyze each individual earthquake because of the very small SN ratio. We analyze the DLF seismicity using the spatio-temporal distributions and waveforms of the DLF earthquakes, as shown in next subsection.

4.2 Classification of DLF earthquakes

To investigate the activations of DLF earthquakes, we attempt to classify the DLF earthquakes. However, it is difficult to classify them based on the relocated hypocenters because most DLF earthquakes are located in the largest cluster at a depth of 22 km (Figure 2). Thus, we classify DLF earthquakes based on the period in which the detected earthquakes are concentrated.

First, to classify template DLF earthquakes, we determine the concentration ratio (CR) of each template earthquake as follows:

$$CR_i(T_{\text{start}}, T_{\text{end}}) = \frac{N_i(T_{\text{start}}<t<T_{\text{end}})}{N_i^{\text{total}}} \quad \cdot\cdot\cdot (2)$$

where N_i^{total} refers to the total number of detected earthquakes by the i th template in all periods of analysis, which is from April 2004 to December 2018. T_{start} and T_{end} show the start times and end times of the periods defined in Table 1. We consider three periods corresponding to the periods of eruptions: December 2009–June 2010 for Type A1, July 2010–September 2011 for Type A2, and September 2017–December 2018 for Type B1. $N_i(T_{\text{start}} < t < T_{\text{end}})$ is the number of detected earthquakes in the period. Then, if CR is over the threshold of each type (see Table 1), the template earthquake is classified into the type. We determine the types of the template earthquakes from the top to the bottom in Table 1. When CRs are not over than thresholds of any type, the template events are classified into Type B2. When a template fits two or more types, the template is classified into the topmost type along Table 1. We do not classify template earthquakes for which less than eight DLF earthquakes were detected. Finally, all detected earthquakes are classified according to the types of the template earthquakes that detected them. In other words, the DLF earthquakes concentrated between December 2009 and

June 2010 are classified into Type A1; those between July 2010 and September 2011 into Type A2 (Figures 5b and c); those which were activated in the period of the 2018 eruptions into Type B1 (Figure 5d); and those occurring constantly from 2004 to 2018 into Type B2 (Figure 5e).

As the result of classification, the number of Type A2 earthquakes is the largest of all types in our classification (Table 1). Additionally, the numbers of Types A1 and B1 are smaller than those of Types A2 and B2. To reveal the causes of these differences, we show the relocated hypocenters in Figure 6. The DLF earthquakes of Type A1 are located around and within the largest cluster at a depth of 22 km and Type A2 are deeper than the other types. Type A2 are separated into three clusters by their spatial distributions (A2.1–A2.3); therefore, we discuss the differences in DLF seismicity in each cluster in subsection 4.3. Types A1 and A2.3 earthquakes are located farther northern than any other type. Types B1 and B2 compose the largest cluster together and are not clearly separated from each other. In addition, some of DLF earthquakes at depths of 12 km are classified into Type B2.

Waveforms of DLF earthquakes have large variations and are complicated. However, the differences in the waveforms between the types are clear. In particular, Type A2 earthquakes have the lowest dominant frequency at approximately 1 Hz, and they show no or small onsets of P waves (Figure 7). The other types (Types A1, B1, and B2) have higher dominant frequencies at approximately 3 Hz and show clear P wave onsets. Furthermore, the earthquakes of Type A1 have a lower dominant frequency than those of Types B1 and B2. Most of the earthquakes of Type A2 clearly have lower dominant frequencies and larger ratios of the amplitudes of S waves to P waves, that is, the typical P wave of Type A2 is weaker than those of the others (Figure 8).

4.3 DLF seismicity in the activation period including the 2011 eruptions

In subsection 4.2, the DLF earthquakes were classified according to time variabilities of the detected earthquakes, and Type A2 were further separated into three clusters (A2.1–A2.3) by their spatial distributions. Thus, we attempt to find differences of DLF seismicity by the clusters.

Small clusters of Type A2 are located at depths of 23 km and 25 km (A2.1–A2.3 in Figure 6). The clusters of A2.1, A2.2, and A2.3 include four, one, and five template DLF earthquakes. The characteristics of temporal DLF activity are different depending on the clusters (Figure 9). In other words, Types A2.1, A2.2, and A2.3 had their own activation periods. As explained above, Types A2.1–A2.3 were first separated based on their spatial distributions but they also differ by the characteristics of time variabilities.

Type A2.1 increased from August 2010 (Figures 9a–c). In two template earthquakes of Type A2.1, three swarms of DLF earthquakes were observed on August 2010, December 2010, and February 2011. Type A2.2 also increased from August 2010 and gradually from December 2010 (Figure 9d). On the other hand, Type A2.3 were observed from December 2010 and activated after the subplinian eruptions (Figures 9e–i).

Figures 10a and 10b show the numbers of DLF earthquakes every 14 days, and the ratios of the earthquakes of Types A1 and A2.1–A2.3. The transitions of the four DLF types are consistent with the changes in eruption styles (Figure 10c). The first stage of the eruption was the phreatic stage from 2008 to July 2010 [Nakada et al., 2013; Suzuki et al., 2013]. In this stage, Type A1 mainly occurred. In August 2010, a swarm of Type A2.1 was observed without eruptions. Although Types A2.2 and A2.3 also appear, those numbers were not large. In December 2010, DLF swarms occurred again and included many earthquakes of Type A2.3 at this time. On January 26–27, 2011, the subplinian eruptions occurred and were followed by lava accumulation events [Nakada et al., 2013], but the number of DLF earthquakes is small.

In this period, the ratio of Type A2.2 is larger than those in the other time periods. Following the subplinian eruptions, vulcanian eruptions and a swarm of DLF earthquakes occurred in February 2011. After the swarm, Type A2.3 increased and lasted until approximately September 2011. From June 2011, phreatomagmatic eruptions occurred and Type A1 increased again. After the eruptions, Types A1 and A2 were not observed.

5 Discussion

5.1 Deep volcanic structure and hypocenters of DLF earthquakes

As explained in section 3, the relocated hypocenters of DLF earthquakes are concentrated in the shallow spot at a depth of 10–15 km and the deep spot at a depth of 20–27 km. Our result shows that the scattering of the hypocenters in each spot is smaller than in the original catalog of the JMA. It should be noted that DLF earthquakes are distributed not continuously, but separately, in a vertical direction. In addition, hypocenters of DLF earthquakes can be separated into some small isolated sources in both shallow and deep spots, based on classification analysis by their seismicity and relocated hypocenters. Vertical discontinuous distributions of DLF earthquakes were also observed at Laacher See volcano in Germany and Iwate volcano in Japan [Nakamichi et al., 2003; Hensch et al., 2019]. Although these previous studies showed 5–20 km scale separation in the vertical discontinuous distribution, our study in Kirishima volcanoes indicated a separation of a few hundred meters. Results in Kirishima volcanoes suggest that many sources of DLF earthquakes are distributed with various separations at spatial scales of a few hundred meters to 10 km. Those vertical isolated distributions of DLF sources are consistent with an idea from petrology of sill-like magma injected in many depths near the Moho discontinuity [Annen et al., 2006; Cashman et al., 2017]. DLF earthquakes may occur around not only vertical conduits but also horizontal sills.

Why DLF earthquakes only occur at these depths is still unclear, but the clue for this question may be the two velocity structure characteristics beneath Kirishima volcanoes. First, Yamamoto and Ida [1994] and Nagaoka et al. [2018] showed a low-velocity zone beneath Kirishima volcanoes using seismic tomography and interferometry. The low-velocity zone is located beneath a depth of 5–15 km. Second, according to Zhao et al. [2018], another low-velocity zone is located between 20 km and 35 km. These two low-velocity zones roughly correspond to the depths of DLF earthquakes. Furthermore, the observations are consistent with the idea that DLF earthquakes occur in or around low-velocity zones and high-attenuation zones in many volcanoes [Hasegawa et al., 2005; Nakajima, 2017; Shina et al., 2018]. Our results suggest that hypocenters of DLF earthquakes are concentrated at many small sources such as magma reservoirs located in the magma sills and conduits in the low velocity zone (Figure 11).

In Kirishima volcanoes, DLF earthquakes have not been observed at 30 km depth, which is equivalent to the Moho discontinuity [Matsubara et al., 2017]. The absence of DLF earthquakes on Moho discontinuity may be explained by one or two of the following two hypotheses. One is that the depth of the Moho discontinuity may locally be shallower than 30 km due to the existence of the volcano. The other is that the density contrast around the Moho discontinuity is small. However, we cannot verify the hypothesis because the resolution of the estimated velocity structure is not sufficiently detailed.

5.2 DLF earthquakes associated with the eruptions

DLF earthquakes in the shallow spot did not increase around the 2011 and 2018 eruptions unlike those in the deep spot (Figure 3d, 3e). Many previous studies proposed the hypothesis that DLF earthquakes are affected by the movement of fluid [Aki and Koyanagi, 1981; Hasegawa et al., 2005; Hotovec-Ellis et al., 2018; Hensch et al., 2019], our results suggest that the fluid movement occurred near the clusters at 20–25 km. Alternatively, no increase in DLF earthquakes in the shallow spot suggests that the fluid did not pass near it. Therefore, one reasonable interpretation of the shallow spot is that it is located along the conduit, connected not to Shinmoe-dake but to Ohachi volcano, which did not erupt in the periods (Figure 11a). This is consistent with the idea of Kagiyama [1994] regarding magnetoelectric and petrological observations that Ohachi volcano can have a different magma supply system from the depth of approximately 20 km. The spatial pattern in the DLF seismicity suggests that the fluid path directly connects to the pressure source at 8 km and the deep spot of DLF earthquakes.

We here discuss the detailed seismicity of the DLF earthquakes in the deep spot corresponding to the 2011 eruptions. The hypocenters of Type A2 are deeper than the others obtained by the NCC method. Type A2 earthquakes may have certainly occurred at approximately 23–25 km, which are deeper than those of the other DLF earthquakes. However, the deep locations of the DLF earthquakes associated with the 2011 eruptions can also be interpreted as follows: these DLF earthquakes occurred at the same depths as the other DLF earthquakes, but they were overestimated due to the possible decrease in P- and S-wave velocities by volcanic activity. However, this interpretation is inconsistent with Type B2, which continuously occurred even during the eruption sequences. Thus, it is reasonable that Type A2 actually occurred at the deep locations.

Type A1 first increased from December 2009 in the period of phreatic eruptions and was followed by the increase in Type A2 before the subplinian eruptions (Figure 10). In this sequence, Type A1 first occurred at a depth of 21.5 km in the period of phreatic eruptions. Next, Types A2.1 were activated at about 23 km without eruptions. Finally, Type A2.2 and A2.3 were activated at approximately 25 km after the subplinian eruptions (Figure 12). These results in the four clusters suggest that the movement of fluid at the depths may have been triggered from shallower part and switched three times with transitions of eruption styles. Therefore, the volcanic activities including such eruptions may have started at the depth shallower than 21 km. In addition, the peak of DLF seismicity appeared after the large crustal deformation triggered by the subplinian eruptions on 26-27 January 2011 (Figure 4). These observation results can be explained by the repressurization of the magma reservoir [Segall, 2016]. Therefore, fluid movement probably started beneath the magma reservoir before the subplinian eruptions. Reduction in pressure, which possibly occurred at the depth of 10–20 km, may have triggered the ascent of fluid from the deep crust. These complex time-variable activities in many depths were also observed at Laacher See volcano [Hensch et al., 2019]. The result in Kirishima volcanoes that DLF seismicity is different even if the hypocenters are close each other provides an idea that there are many fluid paths forming a network and they sometimes switch. In the network of paths, there are some sources of DLF earthquakes such as small magma reservoirs corresponding to magma intrusions. DLF earthquakes are perhaps observed only when the fluid passes near sources such as small magma reservoirs.

While Types A1 and A2 were activated associated with the 2011 eruptions, Type B1 were associated with the 2018 eruptions (see Figure 5d). This result suggests that the fluid path of the 2018 eruptions may have differed from that of the 2011 eruptions (Figure 12e). The dominant frequencies of Type B1 is same as those of type B2. Therefore, low-frequency content of Type A2 may not be attributed to the fluid intrusion or heating but to the structure around the hypocenters of type A2 earthquakes.

The concentration of DLF earthquakes in Kirishima volcanoes suggests that DLF earthquakes occur at specific locations, such as near magma reservoirs. Therefore, we consider a model similar to the trigger and resonant model proposed for volcanic shallow low-frequency earthquakes [Neuberg et al., 2006]. The earthquakes occurred near the surface; however, the waveforms of the shallow low-frequency earthquakes, which have dominant frequencies of approximately 1–10 Hz and a long coda wave, are similar to those of DLF earthquakes. The fluid-filled crack model [Aki et al., 1977], one of the shallow low-frequency earthquake models, can also explain the characteristics of DLF earthquakes. There is a problem as to why earthquakes occur at a depth in which no regular earthquakes have been observed. It may be explained to consider similar model to the cooling magma model in which thermal strain causes brittle failure, and waves are trapped in the resonance [Aso and Tsai, 2014]. If the cooling of magma trigger DLF earthquakes, heating of magma by the fluid flow may also trigger the earthquakes and this model can explain the activation of DLF earthquakes associated with eruptions in Kirishima volcanoes.

5.3 Possibility to predict eruptions by monitoring DLF earthquakes

It is well known that long-period earthquakes, which occur near the surface, are useful for predicting eruptions [Chouet, 1996]. However, if DLF earthquakes are also available, the prediction accuracy will be improved by combining the observations of regular and DLF earthquakes. This study reveals that a large number of unique DLF earthquakes occurred before the 2011 subplinian eruptions and it suggests that monitoring DLF earthquakes may also be useful to predict eruptions in the future. One factor making it difficult to use DLF earthquakes for prediction is their diversity. DLF earthquakes in 2011 and 2018 exhibit many different characteristics of locations and waveforms; hence, we cannot predict at this moment how DLF earthquakes will occur prior to the next eruption. The matched filter technique can only detect the earthquakes that have waveforms and locations similar to those of template earthquakes. Thus, another method not depending on templates is necessary for the prediction.

6 Conclusions

We analyzed DLF earthquakes that occurred at depths of 10–30 km in Kirishima volcanoes and found following features:

1. Relocated hypocenters of DLF earthquakes show that the earthquakes are concentrated in small clusters at the depths of 10–15 km and 20–27 km in low-velocity zones.
2. Activations of DLF earthquakes at depths of 20–27 km associated with the 2011 and 2018 eruptions were observed.
3. The activation with the 2011 eruptions had been observed for approximately two years since December 2009, associated with crustal deformation.
4. Waveforms of the DLF earthquakes associated with the 2011 eruptions had lower dominant frequencies and weak P waves.
5. Most hypocenters of DLF earthquakes associated with the 2011 eruptions were concentrated in four deeper clusters which are different from those of the other earthquakes, and active clusters were switched three times with transitions of eruption styles.
6. The waveforms and hypocenters of DLF earthquakes associated with the 2018 eruptions are almost the same as those of the earthquakes which constantly occurred from 2004 to 2018.

The concentrated locations suggest that DLF earthquakes can occur only in particular locations, such as small magma reservoirs near magma sills. The activations of DLF earthquakes may reflect the fluid flow in the deep crust. In addition, different locations of DLF earthquakes for the 2011 and 2018 eruptions suggest that the fluid paths are different. These results show the possibility that eruption processes are directly related to fluid flow in the deep crust.

Acknowledgments

We used Generic Mapping Tools for drawing figures [Wessel and Smith, 1998] and Hi-net seismic observation data (http://www.hinet.bosai.go.jp) operated by the National Research Institute for Earth Science and Disaster Resilience (NIED) [NIED, 2019]. We used the regional earthquake catalog of the Japan Meteorology Agency (http://www.jma.go.jp). We used GNSS data, F3 solutions provided by Geospatial Information Authority of Japan (http://www.gsi.go.jp). We used the computer systems of the Earthquake and Volcano Information Center of the Earthquake Research Institute, the University of Tokyo. We appreciate Dr. Kazuaki Ohta for providing us the program code of network correlation coefficient method. This research was supported by JSPS KAKENHI Grant Number JP16H06473 in Scientific Research on Innovative Areas "Science of Slow Earthquakes" and Grant Number JP19J12571 in Grant-in-Aid for JSPS Fellows.

References

Aki, K., Fehler, M., & Das, S. (1977). Source mechanism of volcanic tremor: fluid-driven crack models and their application to the 1963 Kilauea eruption. Journal of Volcanology and Geothermal Research, 2(3), 259–287. https://doi.org/10.1016/0377-0273(77)90003-8

Aki, K., & Koyanagi, R. (1981). Deep volcanic tremor and magma ascent mechanism under Kilauea, Hawaii. Journal of Geophysical Research, 86(B8), 7095–7109.

Annen, C., Blundy, J. D., & Sparks, R. S. J. (2006). The genesis of intermediate and silicic magmas in deep crustal hot zones. Journal of Petrology, 47(3), 505–539. https://doi.org/10.1093/petrology/egi084

Aso, N., Ohta, K., & Ide, S. (2013). Tectonic, volcanic, and semi-volcanic deep low-frequency earthquakes in western Japan. Tectonophysics, 600, 27–40. https://doi.org/10.1016/j.tecto.2012.12.015

Aso, N., & Tsai, V. C. (2014). Cooling magma model for deep volcanic long-period earthquakes. Journal of Geophysical Research: Solid Earth, 119(11), 8442–8456. https://doi.org/10.1002/2014JB011180

Cashman, K. V., Sparks, R. S. J., & Blundy, J. D. (2017). Vertically extensive and unstable magmatic systems: A unified view of igneous processes. Science, 355(6331). https://doi.org/10.1126/science.aag3055

Chouet, B. A. (1996). Long-period volcano seismicity: its source and use in eruption forecasting. Nature, 380(6572), 309–316. https://doi.org/10.1038/380309a0

Frank, W. B., Shapiro, N. M., & Gusev, A. A. (2018). Progressive reactivation of the volcanic plumbing system beneath Tolbachik volcano (Kamchatka, Russia) revealed by long-period seismicity. Earth and Planetary Science Letters, 493, 47–56. https://doi.org/10.1016/j.epsl.2018.04.018

Funasaki, J., & Earthquake Prediction Information Division. (2004). Revision of the JMA velocity magnitude. Quarterly Journal of Seismology, 67(1–4), 11–20. (in Japanese with English abstract)

Gibbons, S. J., & Ringdal, F. (2006). The detection of low magnitude seismic events using array-based waveform correlation. Geophysical Journal International, 165: 149–166. https://doi.org/10.1111/j.1365-246X.2006.02865.x

Hasegawa, A., Nakajima, J., Umino, N., & Miura, S. (2005). Deep structure of the northeastern Japan arc and its implications for crustal deformation and shallow seismic activity. Tectonophysics, 403(1–4), 59–75. https://doi.org/10.1016/j.tecto.2005.03.018

Hensch, M., Dahm, T., Ritter, J., Heimann, S., Schmidt, B., Stange, S., & Lehmann, K. (2019). Deep low-frequency earthquakes reveal ongoing magmatic recharge beneath Laacher See Volcano (Eifel, Germany). Geophysical Journal International, 216(3), 2025–2036. https://doi.org/10.1093/gji/ggy532

Hotovec-Ellis, A. J., Shelly, D. R., Hill, D. P., Pitt, A. M., Dawson, P. B., & Chouet, B. A. (2018). Deep fluid pathways beneath Mammoth Mountain, California, illuminated by migrating earthquake swarms. Science Advances, 4(8), eaat5258. https://doi.org/10.1126/sciadv.aat5258

Japan Meteorology Agency (2018). Volcanic activity of Kirishimayama volcano –February 1, 2018 – May 31, 2018–. Report of Coordinating Committee for Prediction of Volcanic Eruption, 130, 213-284. (in Japanese)

Kagiyama, T. (1994). Kirishima volcanoes – Multi active volcanic group generated in a slightly tensile stress field. Journal of Geography, 103(5), 479–487. (in Japanese with English abstract)

Katsumata, A., & Kamaya, N. (2003). Low-frequency continuous tremor around the Moho discontinuity away from volcanoes in the southwest Japan. Geophysical Research Letters, 30(1), 1020. https://doi.org/10.1029/2002GL015981

Kosuga, M., Noro, K., & Masukawa, K. (2017). Characteristics of spatiotemporal variations of hypocenters and diversity of waveforms of deep low-frequency earthquakes in northeastern Japan. Bulletin of the Earthquake Research Institute, University of Tokyo, 92, 63–80. (in Japanese with English abstract)

Matsubara, M., Sato, H., Ishiyama, T., & Van Horne, A.D. (2017). Configuration of the Moho discontinuity beneath the Japanese Islands derived from three-dimensional seismic tomography. Tectonophysics, 710–711, 97–107, https://doi.org/10.1016/j.tecto.2016.11.025

Nagaoka, Y., Nishida, K., Aoki, Y., Takeo M., Ohkura S., & Yoshikawa, S. (2018). V_{SV} and V_{SH} structure beneath Kirishima volcanoes inferred from seismic interferometry. Japan Geophysical Union Meeting 2018, SVC41-44 (Abstract)

Nakada, S., Nagai, M., Kaneko, T., Suzuki, Y., & Maeno, F. (2013). The outline of the 2011 eruption at Shinmoe-dake (Kirishima), Japan. Earth, Planets and Space, 65(6), 475–488. https://doi.org/10.5047/eps.2013.03.016

Nakajima, J. (2017). Seismic velocity and attenuation structures around active volcanoes beneath Tohoku: Linking Crustal Structure to Low-frequency Earthquakes and S-wave Reflectors. Bulletin of the Earthquake Research Institute, University of Tokyo, 92, 49–62. (in Japanese with English abstract)

Nakamichi, H., Hamaguchi, H., Tanaka, S., Ueki, S., Nishimura, T., & Hasegawa, A. (2003). Source mechanisms of deep and intermediate-depth low-frequency earthquakes beneath Iwate volcano, northeastern Japan. Geophysical Journal International, 154(3), 811–828. https://doi.org/10.1046/j.1365-246X.2003.01991.x

Nakamichi, H., Yamanaka, Y., Terakawa, T., Horikawa, S., Okuda, T., & Yamazaki, F. (2013). Continuous long-term array analysis of seismic records observed during the 2011 Shinmoedake eruption activity of Kirishima volcano, southwest Japan. Earth, Planets and Space, 65(6), 551–562. https://doi.org/10.5047/eps.2013.03.002

Nakao, S., Morita, Y., Yakiwara, H., Oikawa, J., Ueda, H., Takahashi, H., Ohta, Y., Matsushima, T., & Iguchi, M. (2013). Volume change of the magma reservoir relating to the 2011 Kirishima Shinmoe-dake eruption—Charging, discharging and recharging process inferred from GPS measurements. Earth, Planets and Space, 65(6), 505–515. https://doi.org/10.5047/eps.2013.05.017

National Research Institute for Earth Science and Disaster Resilience (2019). NIED Hi-net, https://doi.org/10.17598/nied.0003

Neuberg, J. W., Tuffen, H., Collier, L., Green, D., Powell, T., & Dingwell, D. (2006). The trigger mechanism of low-frequency earthquakes on Montserrat. Journal of Volcanology and Geothermal Research, 153(1–2), 37–50. https://doi.org/10.1016/j.jvolgeores.2005.08.008

Ohta, K., & Ide, S. (2011). Precise hypocenter distribution of deep low-frequency earthquakes and its relationship to the local geometry of the subducting plate in the Nankai subduction zone, Japan. Journal of Geophysical Research, 116, B01308. https://doi.org/10.1029/2010JB007857

Okada, Y., Kasahara, K., Hori, S., Obara, K., Sekiguchi, S., Fujiwara, H., & Yamamoto, A. (2004). Recent progress of seismic observation networks in Japan —Hi-net, F-net, K-NET and KiK-net—. Earth, Planets and Space, 56(8), xv–xxviii. https://doi.org/10.1186/BF03353076

Sagiya, T. (2004). A decade of GEONET: 1994-2003 - The continuous GPS observation in Japan and its impact on earthquake studies -. Earth, Planets and Space, 56(8), xxix–xli. https://doi.org/10.1186/BF03353077

Segall, P. (2016). Repressurization following eruption from a magma chamber with a viscoelastic aureole. Journal of Geophysical Research: Solid Earth, 121(12), 8501–8522. https://doi.org/10.1002/2016JB013597

Shapiro, N. M., Droznin, D. V, Droznina, S. Y., Senyukov, S. L., Gusev, A. A., & Gordeev, E. I. (2017). Deep and shallow long-period volcanic seismicity linked by fluid-pressure transfer. Nature Geoscience, 10(6), 442–445. https://doi.org/10.1038/ngeo2952

Shelly, D. R., Beroza, G. C., & Ide, S. (2007). Non-volcanic tremor and low-frequency earthquake swarms. Nature, 446(7133), 305–307. https://doi.org/10.1038/nature05666

Shiina, T., Takahashi, H., Okada, T., & Matsuzawa, T. (2018). Implications of seismic velocity structure at the junction of Kuril-Northeastern Japan arcs on active shallow seismicity and deep low-frequency earthquakes. Journal of Geophysical Research: Solid Earth, 123(10), 8732–8747. https://doi.org/10.1029/2018JB015467

Suzuki, Y., Nagai, M., Maeno, F., Yasuda, A., Hokanishi, N., Shimano, T., Ichihara, M., Keneko, T., & Nakada, S. (2013). Precursory activity and evolution of the 2011 eruption of Shinmoe-dake in Kirishima volcano—insights from ash samples. Earth, Planets and Space, 65(6), 591–607. https://doi.org/10.5047/eps.2013.02.004

Takahashi, H., & Miyamura, J. (2009). Deep Low-Frequency Earthquakes occurring in Japanese Islands. Geophysical Bulletin of Hokkaido University, 72, 177–190. (in Japanese with English abstract)

Ukawa, M. (2007). Low frequency earthquakes at Mount Fuji. Fuji Volcano, 161–172. (in Japanese with English abstract)

Ukawa, M., & Ohtake, M. (1987). A monochromatic earthquake suggesting deep-seated magmatic activity beneath the Izu-Ooshima Volcano, Japan. Journal of Geophysical Research, 92(10), 12,649-12,663. https://doi.org/10.1029/JB092iB12p12649

Wessel, P., & Smith, W. H. F. (1998). New, improved version of Generic Mapping Tools released. Eos, Transactions American Geophysical Union, 79(47), 579. https://doi.org/10.1029/98EO00426

White, R. A. (1996). Precursory deep long-period earthquakes at Mount Pinatubo: Spatio-temporal link to a basalt trigger. University of Washington Press, Seattle, Fire and Mud: Eruptions and Lahars of Mount Pinatubo, Philippines. Newhall, C.G., Punongbayan, R.S. (Eds.), 307–326.

Yamamoto, K., & Ida, Y. (1994). Three-dimensional P-wave velocity structure of Kirishima volcanoes using regional seismic events. Bulletin of the Earthquake Research Institute, University of Tokyo, 69, 267–289. (in Japanese with English abstract)

Zhao, D., Yamashita, K., & Toyokuni, G. (2018). Tomography of the 2016 Kumamoto earthquake area and the Beppu-Shimabara graben. Scientific Reports, 8(1), 15488. https://doi.org/10.1038/s41598-018-33805-0

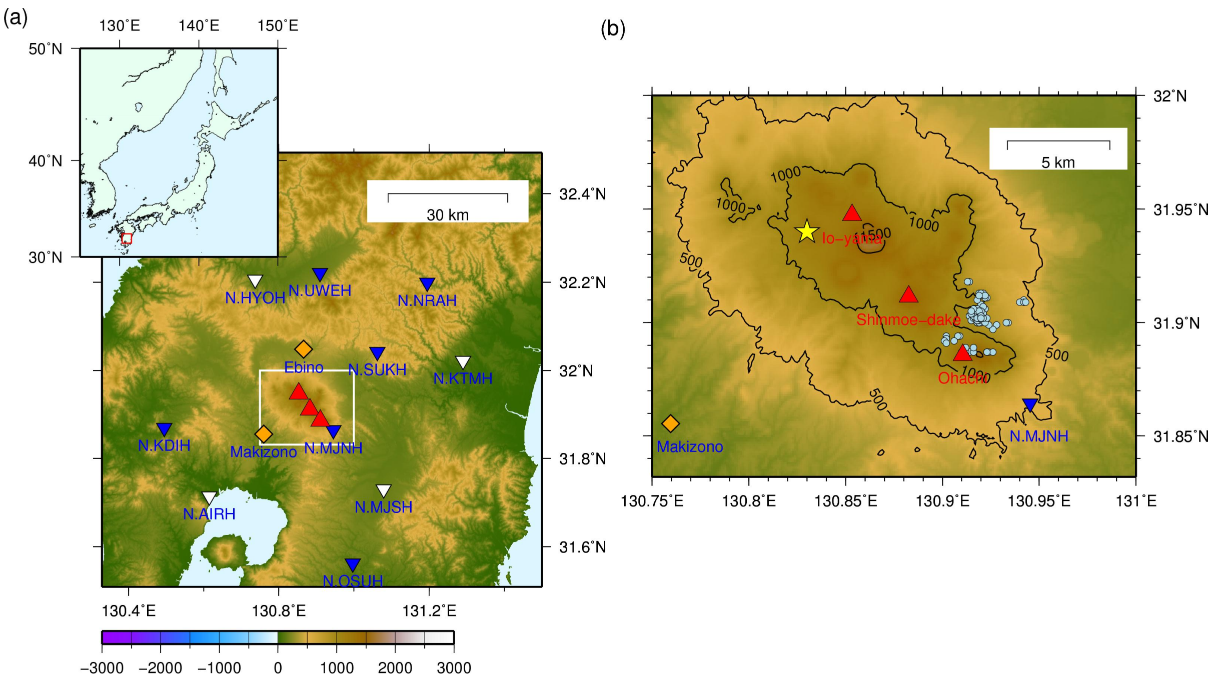

Figure 1. (a) Locations of Kirishima volcanoes and observation stations used in this study. Red triangles show the locations of Io-yama, Shinmoe-dake, and Ohachi volcanoes in Kirishima volcanoes. Inversed triangles indicate the locations of Hi-net stations used for relocation and detection (blue) and used only for relocation (white). N.KTMH and N.AIRH stations are also used for detection when one or two blue stations are missing observations.

Orange diamonds show the locations of global navigation satellite system (GNSS) stations in GNSS earth observation network system (GEONET) [Sagiya, 2004] operated by Geospatial Information Authority of Japan. (b) Enlarged view in the white rectangle in (a) with the same symbols. In addition, light blue circles show the locations of DLF earthquakes obtained by the relocation discussed in section 3. A yellow star represents the location of the estimated pressure source of the 2011 Shinmoe-dake eruptions at the depths of approximately 8 km [Nakao et al., 2013].

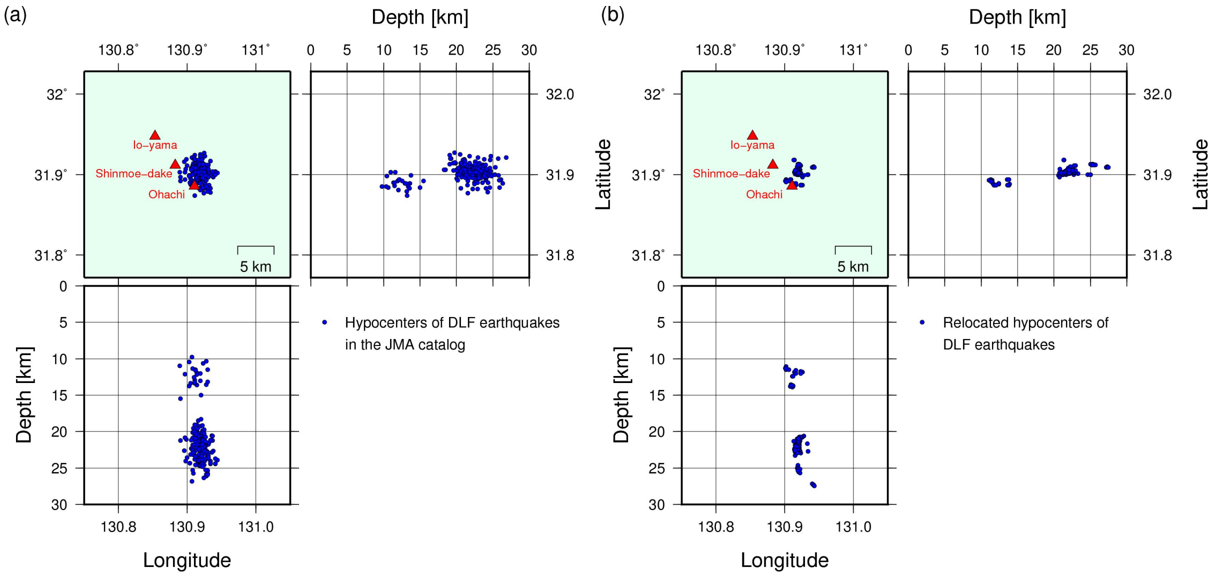

Figure 2. (a) Three-dimensional distributions of DLF earthquakes in the JMA catalog. Red triangles are the summits of three active volcanoes in the Kirishima volcanoes. Blue circles show the locations of DLF earthquakes, which can be relocated by NCC method. (b) Three-dimensional distribution of the earthquakes after relocation.

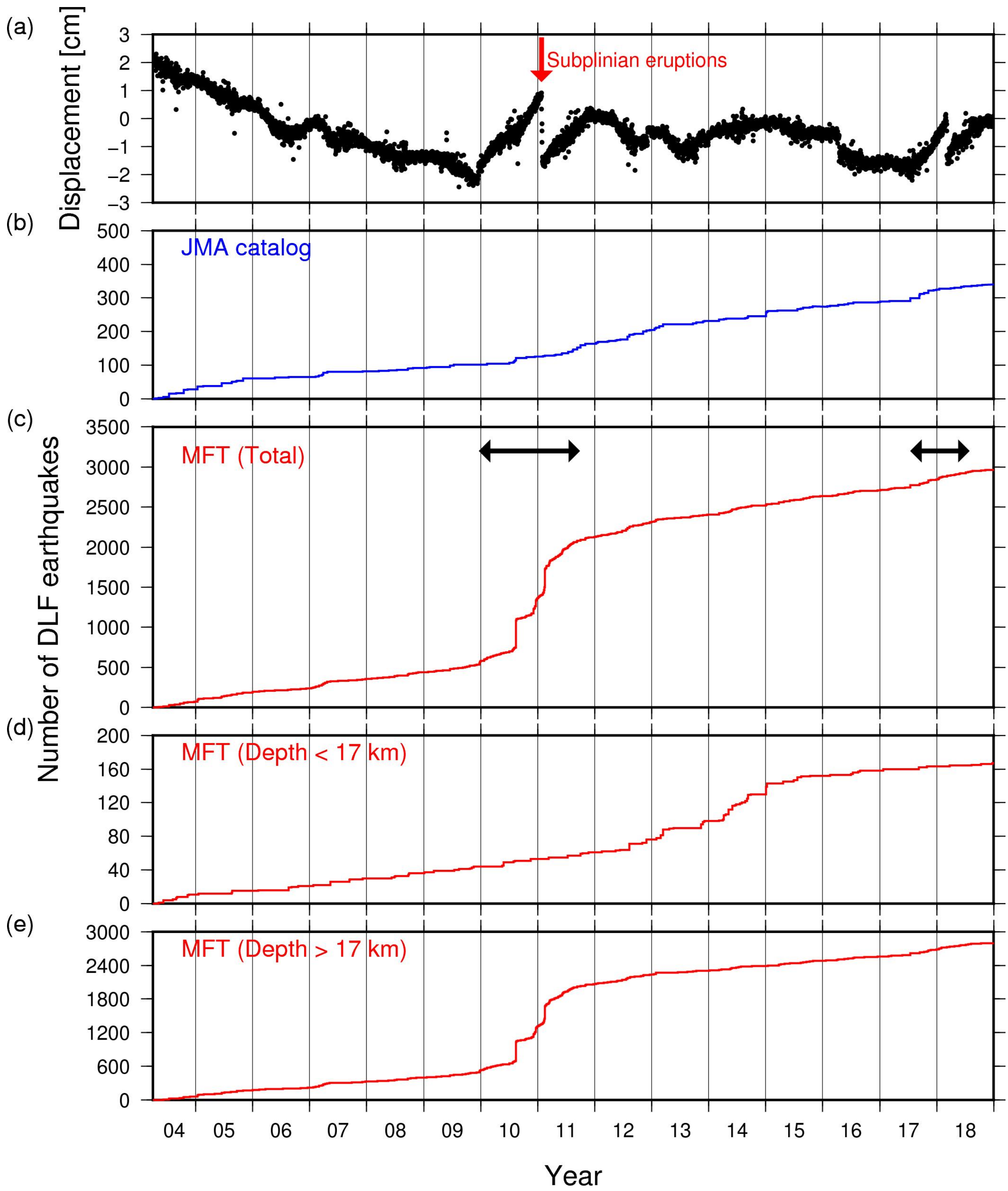

Figure 3. (a) The amount of the horizontal displacement of Ebino relative to Makizono (see Figure 1) calculated from GNSS data. We use F3 solutions provided by Geospatial Information Authority of Japan. (b) A cumulative number of DLF earthquakes in the JMA catalog from April 2004. (c) Cumulative number of DLF earthquakes detected by the matched filter technique (MFT). Black arrows show periods of increasing DLF earthquakes. (d) Cumulative number of DLF earthquakes detected by MFT located shallower than 17 km. (e) Cumulative number of DLF earthquakes detected by MFT located deeper than 17 km.

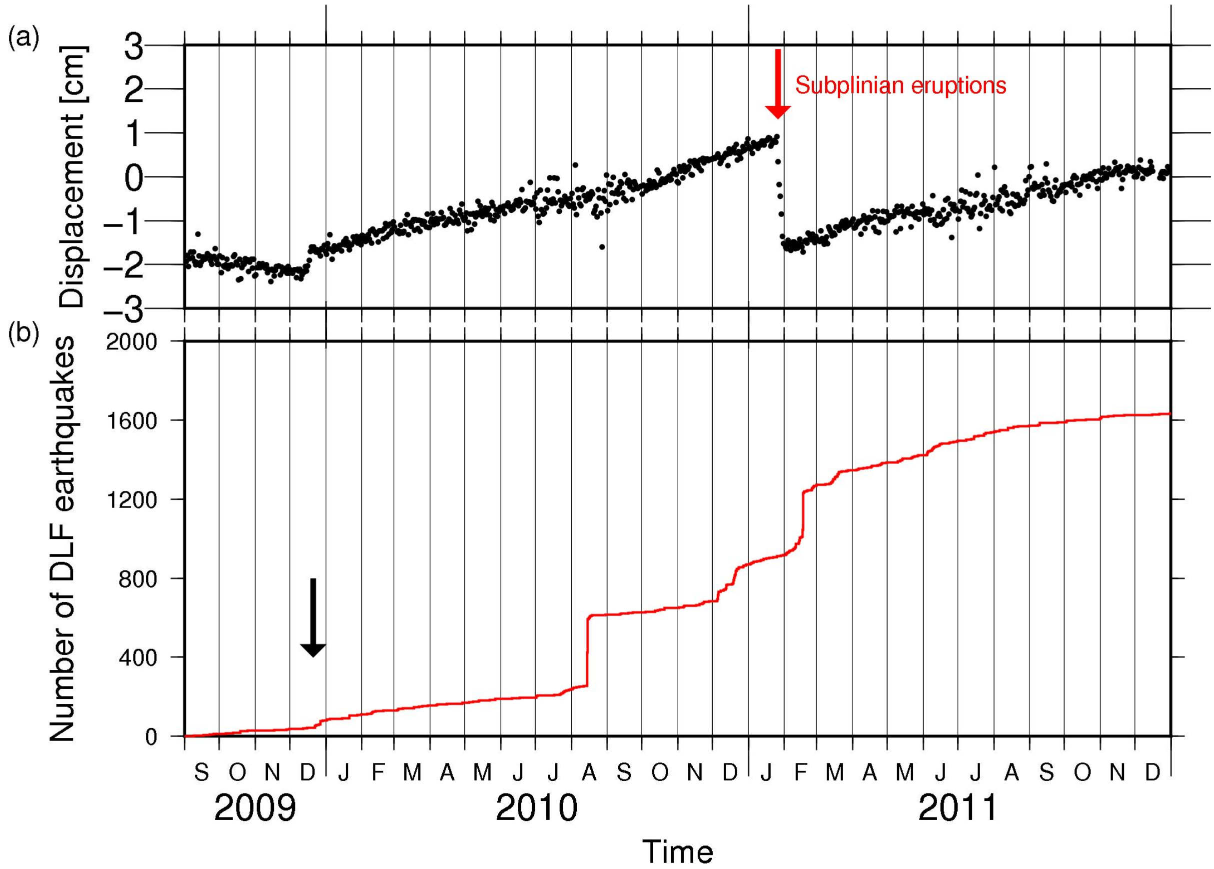

Figure 4. The enlarged portions of Figures 3a and 3c from September 2009 to December 2011. The black arrow shows when increasing of DLF earthquakes initiated.

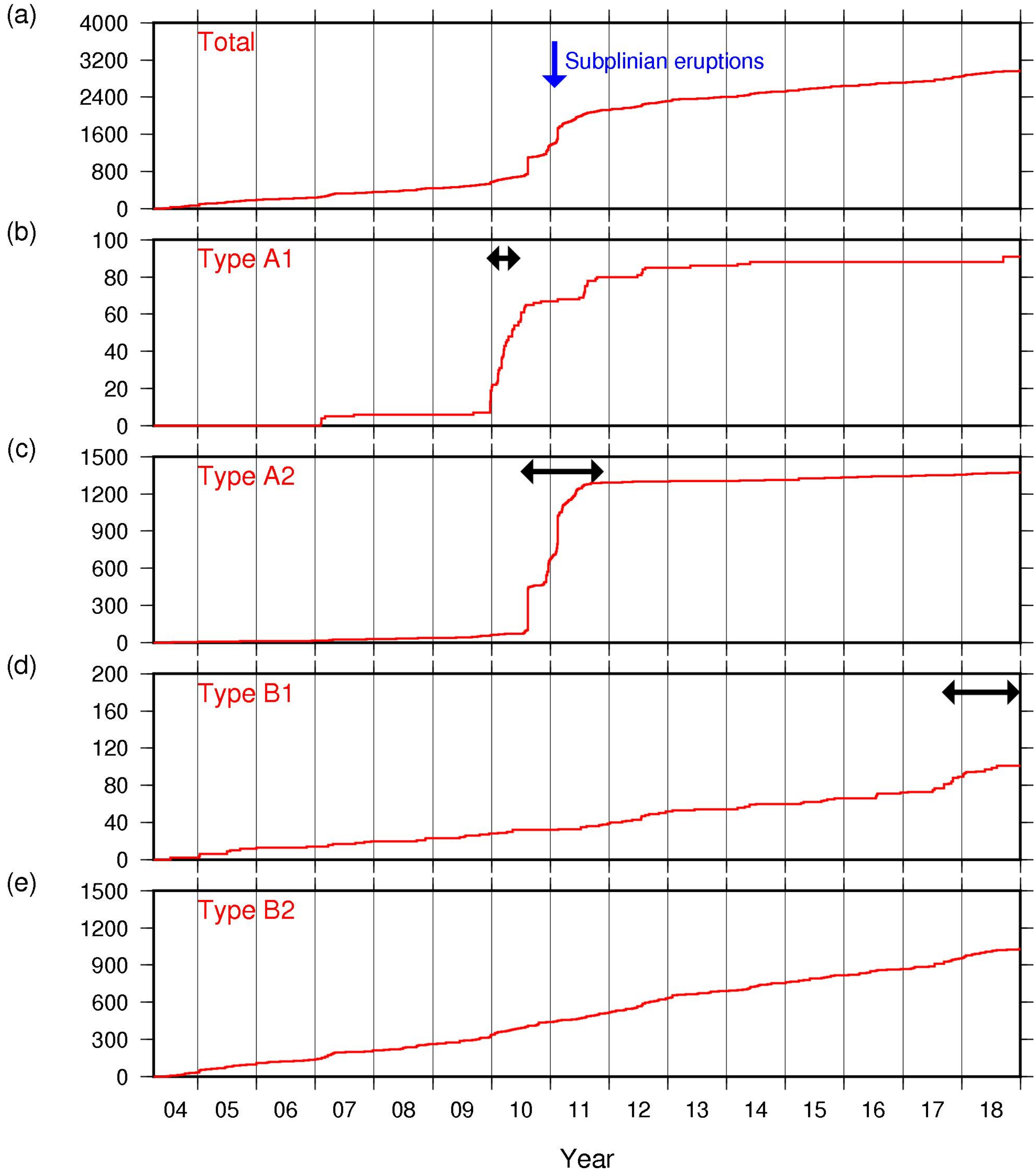

683
684 Figure 5. Cumulative number of DLF earthquakes. (a) Same figure as Figure 3c. (b–e)
685 Total cumulative number of DLF earthquakes classified into each type. Black arrows show the
686 periods in which each type earthquakes are concentrated.

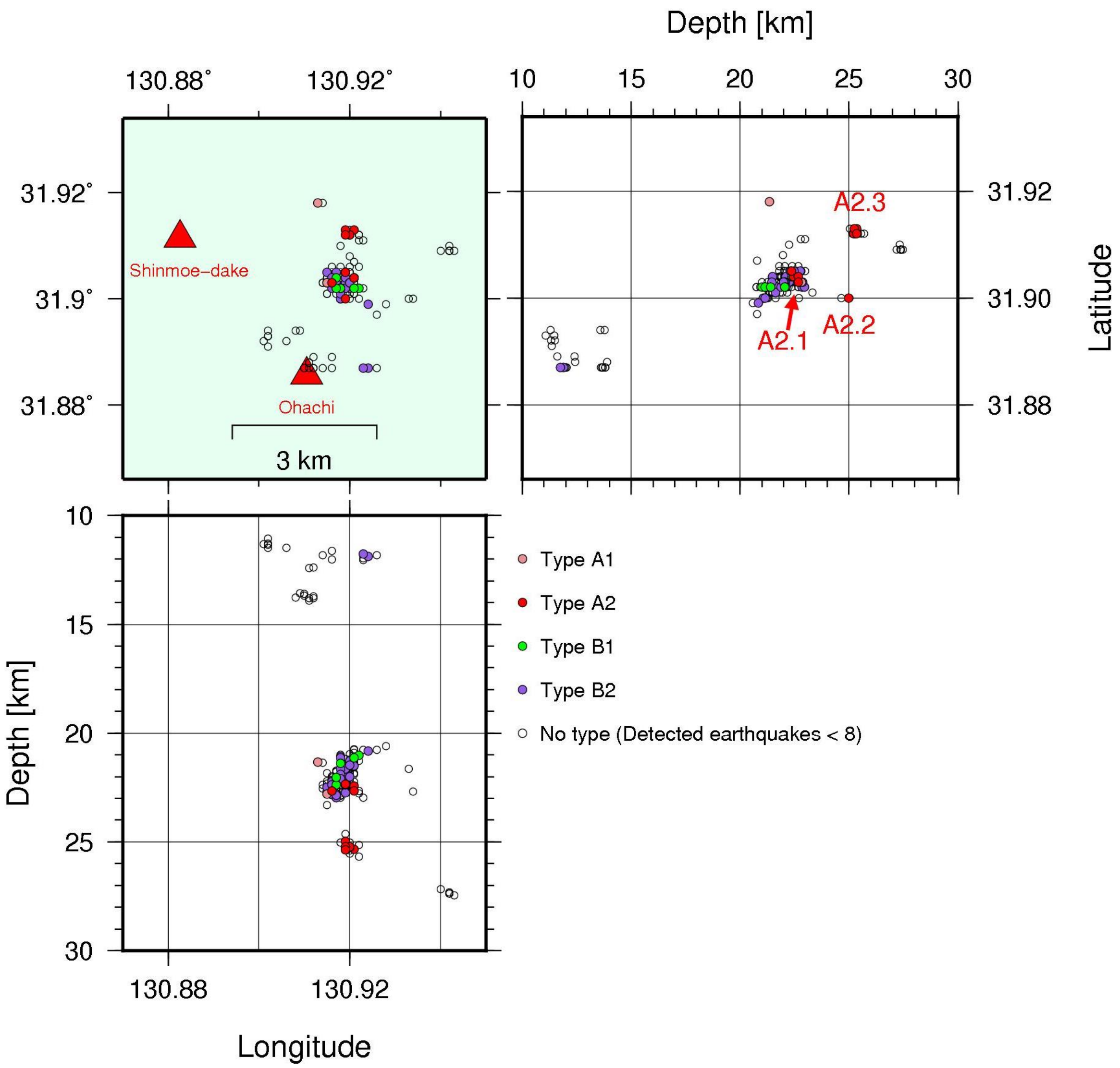

Figure 6. Three-dimensional distribution of DLF earthquakes. The circles indicate the relocated hypocenters of DLF earthquakes, and the colors of the circles show the types of earthquakes (see Table 1). Red triangles represent the summits of Shinmoe-dake and Ohachi volcanoes. White circles are the relocated but unclassified hypocenters of DLF earthquakes, for which fewer than eight earthquakes were detected. A2.1–A2.3 show the locations of Type A2 earthquakes discussed in subsection 4.3.

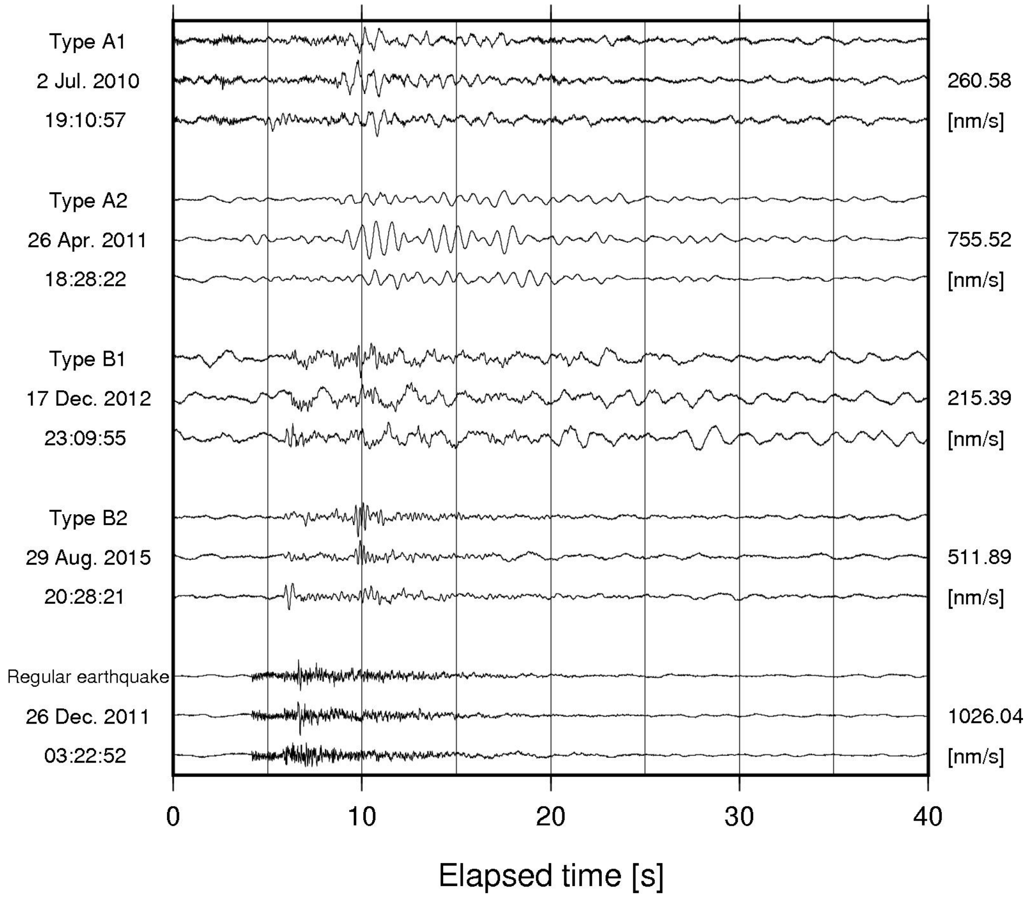

Figure 7. Three components of typical velocity waveforms of each type of DLF earthquake and a regular earthquake observed at the N.SUKH station (see Figure 1). The three waveforms correspond to the east-west, north-south, and up-down components from the top. The type of DLF earthquake and occurrence time (Japan standard time) are written to the left of the waveforms. All waveforms are normalized by the maximum amplitudes of each earthquake written in right. A bandpass filter is not applied to the waveforms.

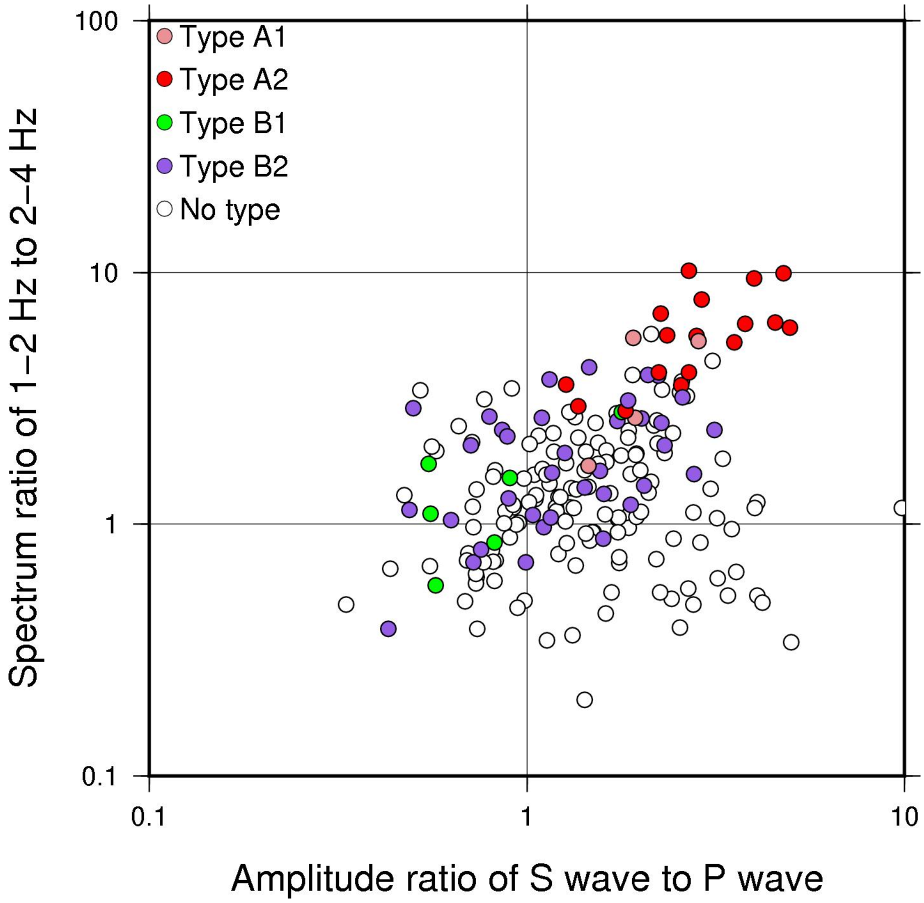

Figure 8. Distribution of the maximum amplitude ratios of S waves to P waves and the ratios of the average spectrum of 1–2 Hz to 2–4 Hz at N.SUKH station. The circles show the DLF earthquakes, and the colors indicate the types of the earthquakes listed in Table 1.

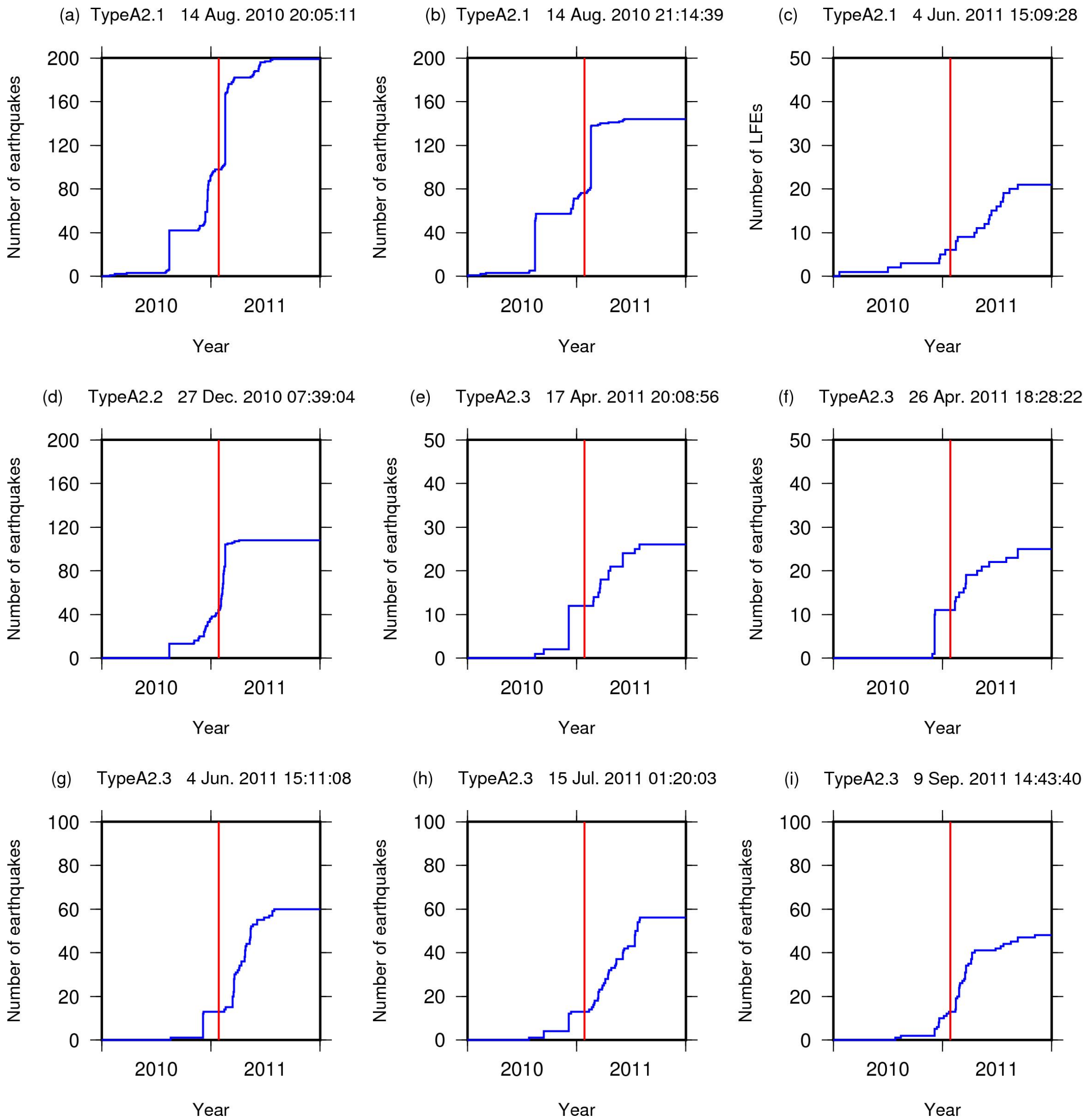

Figure 9. Cumulative number of DLF earthquakes detected by each template earthquake of Type A2 from January 2010, except the template which detected less than 20 earthquakes. Type and occurrence time of each template earthquake are written above the figures. Red lines show the time of the subplinian eruptions of Shinmoe-dake on 26 January 2011.

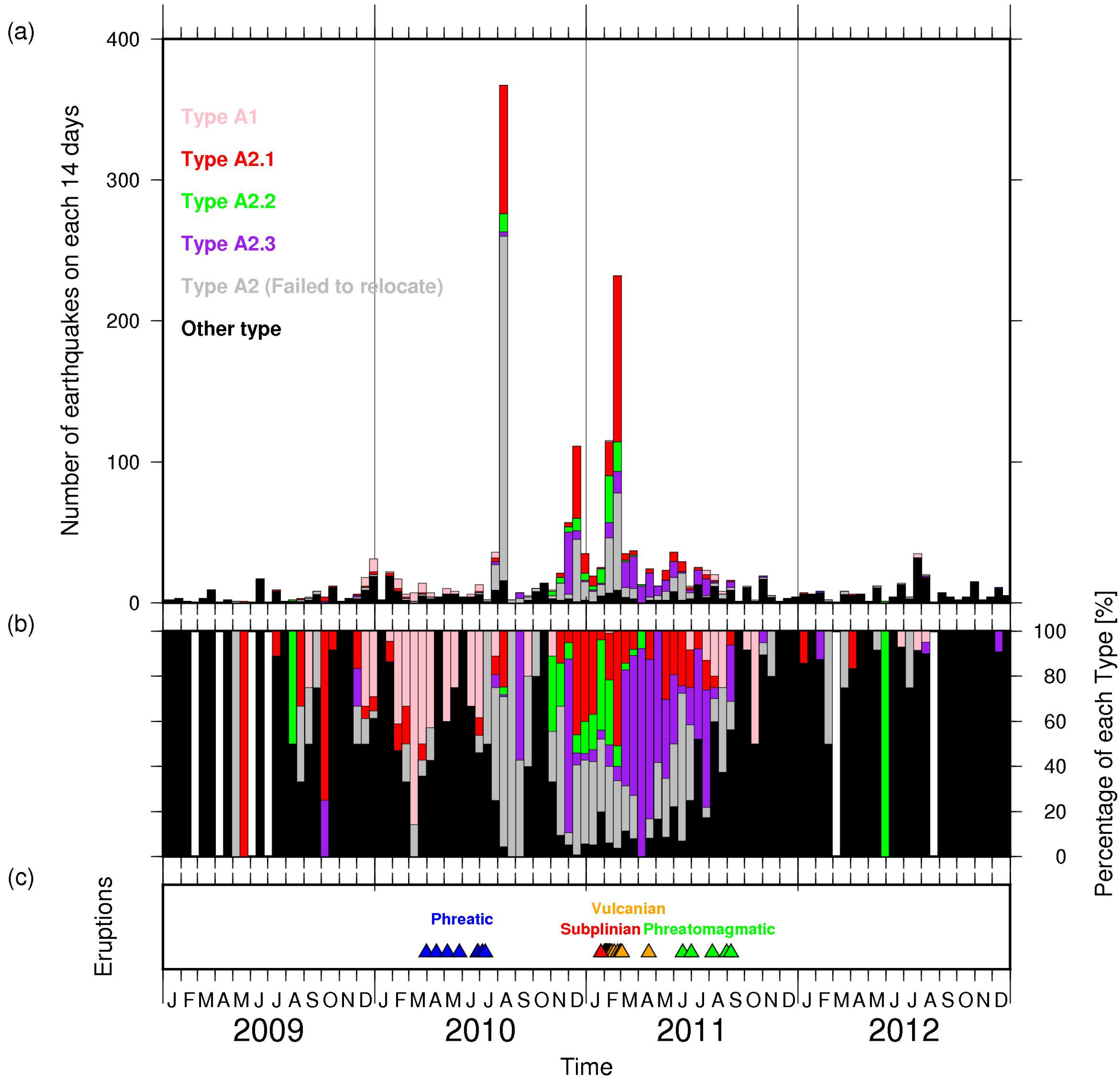

Figure 10. (a) Number of DLF earthquakes in a 14-days time window. Bars show the number of earthquakes, and their colors indicate the types of the earthquakes. (b) Percentages of each type of DLF earthquakes. White lines show the absence of earthquakes in a 14-days time window. (c) The transition of the eruptions of Shinmoe-dake volcano. The times of the eruptions were reported in Nakada et al. [2013]. Eruption stages of less than a few days were excluded.

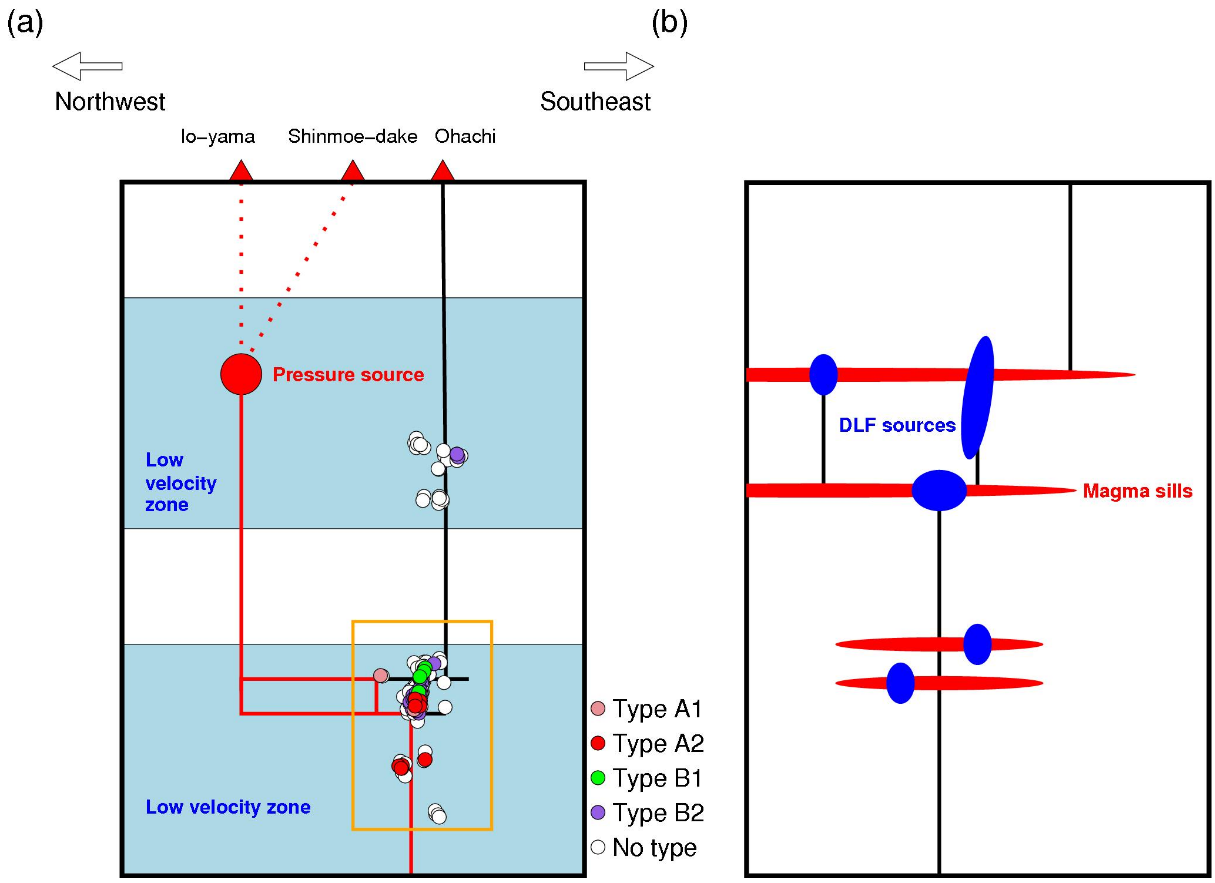

Figure 11. (a) Schematic model of volcanic fluid paths inferred from hypocenters of DLF earthquakes and interaction between DLF earthquakes and surface volcanic activities. A large red circle is the magma reservoir [Nakao et al., 2013]. Colored small circles are hypocenters of DLF earthquakes and the colors show the types of DLF earthquakes as Figures 6 and 8. Red dotted lines represent the conduits for Shinmoe-dake [Nakamichi et al., 2013] and Io-yama from the magma reservoir. Black and red solid lines indicate the estimated paths of magma for the volcanoes based on DLF seismicity. Red lines show the estimated active paths at the 2011 eruptions and black lines show the estimated paths that were not active at the 2011 eruptions. Blue hatches show the low-velocity zone reported in previous studies [Yamamoto and Ida, 1994; Nagaoka et al., 2018; Zhao et al., 2018]. (b) Enlarged model of the fluid paths and magma sills near DLF sources. The area is shown as the orange rectangle in (a). Red horizontal lines show the magma sills and vertical lines show conduits. Blue ellipses show the sources of DLF earthquakes such as magma reservoirs.

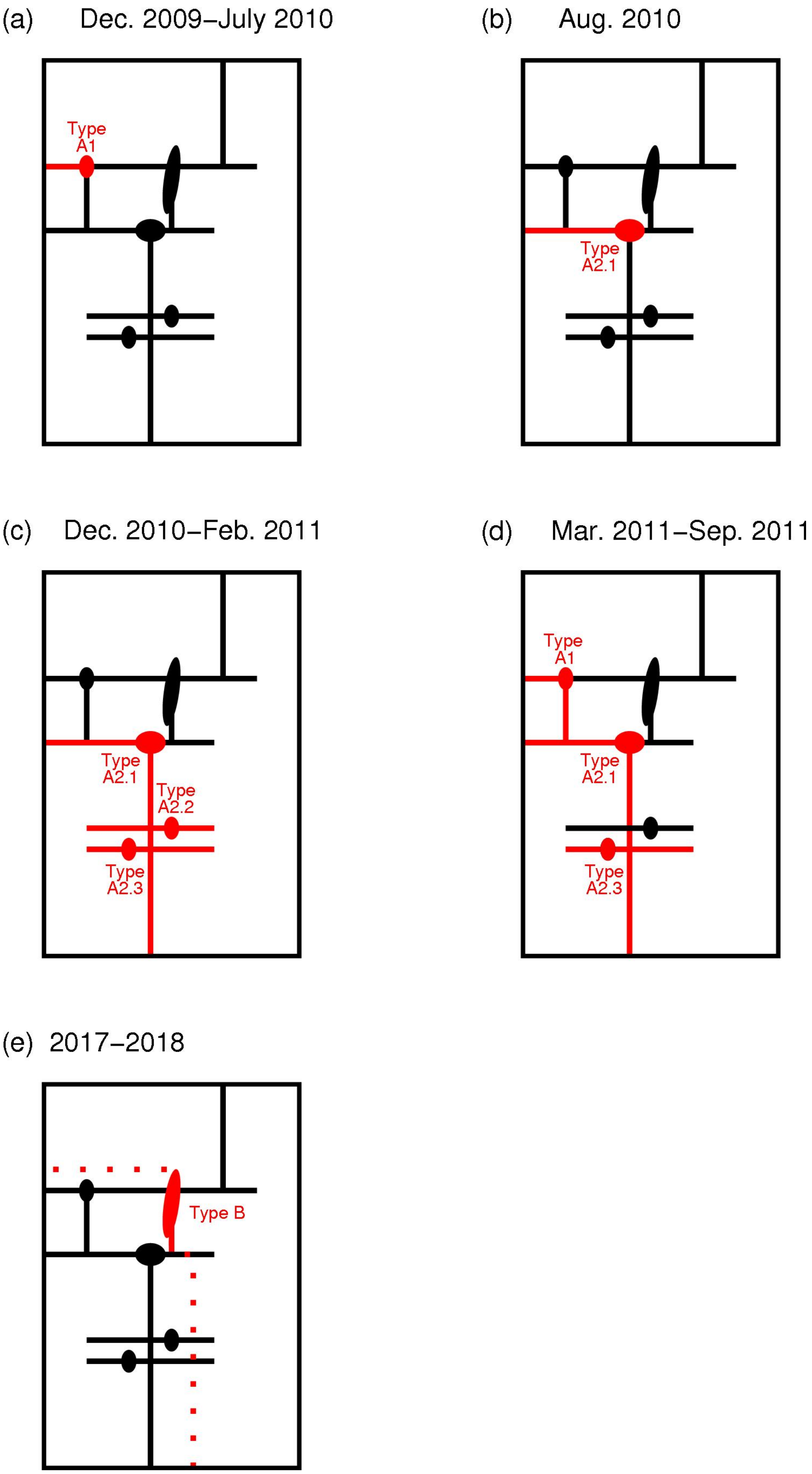

Figure 12. Distribution of DLF earthquakes and estimated fluid flow paths on each term, in which swarms or increases in DLF earthquakes occurred. (a)–(d) are in terms of the 2011 eruptions, December 2009–July 2010, August 2010, December 2010–February 2011, and

March 2011–September 2011, respectively, and (e) for the 2017–2018 eruptions. The area is same as Figure 11(b). Red and black lines show the active and non-active paths of fluid estimated from the activities of DLF earthquakes in each term, respectively. Red dotted lines in (e) show imaginary magma paths in the period of 2017–2018 eruptions. Ellipses show the sources of DLF earthquakes such as magma reservoirs.

Table 1. Definition and number of each type of DLF earthquakes.

Type of DLF earthquakes	Periods	Thresholds of CR	Number of template earthquakes (Relocated earthquakes)	Number of detected earthquakes
A1	December 2009-June 2010	0.4	4 (2)	91
A2	July 2010-September 2011	0.4	17 (10)	1373
B1	September 2017-December 2018	0.2	6 (6)	101
B2	All template earthquakes except above		36 (32)	1027
No type	Detected earthquakes < 8 or not used for MFT		212 (152)	372